International Journal of Microwave and Wireless Technologies

cambridge.org/mrf

Wideband double-layer reflectarray antenna employing subwavelength multi-resonant elements for C-band application

Yunlong Wu, Zhiyuan Yang and Yufeng Liu

School of Physics and Electronic Engineering, Shanxi University, Shanxi, China

Research Paper

Cite this article: Wu Y, Yang Z, Liu Y (2026) Wideband double-layer reflectarray antenna employing subwavelength multi-resonant elements for C-band application. *International Journal of Microwave and Wireless Technologies* **18**(2), 332–344. https://doi.org/10.1017/S1759078726103390

Received: 23 January 2026 UTC
Revised: 16 May 2026 UTC
Accepted: 22 May 2026 UTC

Keywords:
frequency selective surface; reflectarray antenna; reflection phase; tri-band

Corresponding author: Yufeng Liu;
Email: liuyufeng@sxu.edu.cn

Abstract

This paper presents a wideband C-band reflectarray antenna based on subwavelength triple-resonant phase engineering to address the inherent bandwidth limitation of conventional single-resonant reflectarrays. The proposed unit cell, with a compact size of $0.33\lambda_0$ (where λ_0 is the free-space wavelength at the center frequency) at 6.2 GHz, employs a double-layer configuration composed of two PTFE substrates (relative permittivity $\varepsilon_r = 2.55$) separated by a 3-mm air gap and printed with three metallic layers. By deliberately introducing three staggered resonances through arc delay-lines, Koch-fractal loops, and cross-shaped resonators, the reflection-phase dispersion is significantly flattened across 4.76–6.70 GHz. Unlike tightly coupled or three-dimensional reflectarrays that enhance bandwidth at the expense of structural complexity, the proposed design achieves broadband operation through systematic phase-slope control while maintaining a planar and fabrication-friendly architecture. An 11 × 11 prototype with a 200 mm × 200 mm aperture was fabricated and fed by a broadband log-periodic dipole antenna to ensure stable aperture illumination. Measured results demonstrate a 3-dB gain bandwidth of 19%, a peak gain of 19.9 dBi at 6.2 GHz, sidelobe levels below −12 dB, and cross-polarization below −29 dB across the operating band. The proposed approach provides an effective and compact solution for broadband C-band reflectarrays through phase-dispersion engineering rather than structural enlargement or complex feeding networks.

Introduction

Reflectarray antennas (RAs) have attracted extensive research interest due to their low profile, high gain, lightweight structure, and ease of fabrication. Combining the advantages of parabolic reflectors and phased arrays, reflectarrays employ a spatial feed system instead of a complex feed network, effectively minimizing distribution losses while providing flexible beam-shaping capabilities through element-wise phase control [1–4]. These attributes make them excellent candidates for modern satellite communication, radar sensing, and wireless power transmission systems where compactness and efficiency are essential.

However, the operational bandwidth of conventional reflectarrays is typically narrow, mainly limited by the frequency-dependent reflection phase characteristics of individual elements [5]. The phase response of most patch-type elements varies nonlinearly with frequency, resulting in phase errors across the aperture and degraded radiation performance. Achieving broadband operation therefore requires innovative unit-cell designs capable of maintaining linear phase variation and stable reflection amplitude over a wide frequency range.

Recent research has explored various strategies to mitigate the inherent bandwidth limitations of RAs. Adjusting the size, shape, and arrangement of reflective elements has proven effective in enhancing bandwidth performance. For example, wideband, tightly coupled dipole reflectarrays using three-dimensional (3D) elements placed in close proximity have been introduced [6, 7]. This arrangement enhances inter-element coupling, thereby extending operational bandwidth. For instance, a tightly coupled reflectarray reported by Wu et al. [7] achieves an ultra-wide operating bandwidth of 90%. However, it significantly increases design complexity and manufacturing costs. Additionally, other studies [8, 9] have adopted multi-resonant reflectarray elements that introduce supplementary resonances, enhancing phase linearity and broadening the frequency response. Despite these improvements, multi-resonant structures inherently add complexity to antenna designs. Alternatively, subwavelength unit cells enable multiple elements to be integrated within a half-wavelength spacing, thereby improving phase compensation accuracy and broadening the achievable bandwidth [9–12]. Extending this concept, a 1-bit reconfigurable reflectarray based on polarization-rotating unit cells achieves a unit-cell bandwidth of about 30% and a corresponding 3-dB gain bandwidth exceeding 30% for

© The Author(s), 2026. Published by Cambridge University Press in association with The European Microwave Association.

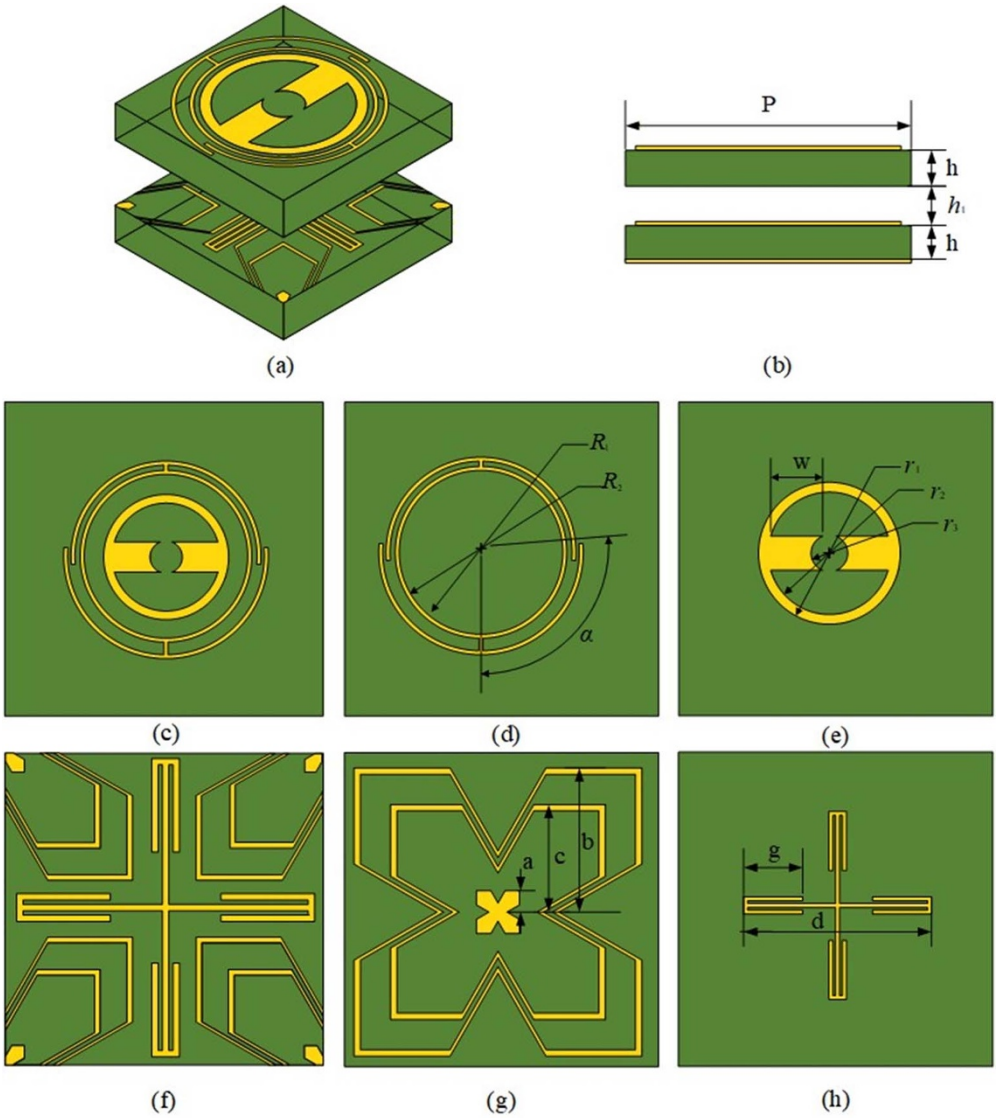


Figure 1. (a) Unit stereogram. (b) Unit side view. (c) Upper-layer unit structure composition. (d) Higher-frequency reflective elements. (e) Frequency-selective surface elements. (f) Lower-layer unit structure composition. (g) Medium-frequency reflective elements. (h) Low-frequency reflective elements.

a fixed beam state [10]. Similarly, a dual-circularly-polarized multi-beam reflectarray employing a subwavelength shared-aperture configuration achieves a 3-dB gain bandwidth of approximately 20% in the Ka-band [11], demonstrating the potential of subwavelength techniques for broadband multi-beam and dual-polarized applications. Another approach applies encoded metasurface theory to reflective surfaces. However, encoded reflective elements typically provide limited phase resolution, which can degrade radiation performance, reduce directivity, and lower aperture efficiency. Moreover, broadband operation may introduce frequency-dependent beam distortion, leading to beam squinting or pointing deviations and making it difficult to maintain stable radiation characteristics across a wide bandwidth. The C band is widely used in satellite communications due to its favorable propagation characteristics [13]. RAs have emerged as high-gain antennas for long-distance communications. Conventional parabolic reflector antennas are widely used for satellite links; however, small satellite platforms have limited payload capacity for bulky reflector antennas [14]. In a reflectarray, each element controls the phase of the reflected wave to synthesize the desired radiation beam.

Table 1. Structural parameters of the proposed reflectarray element

Parameters	P	h	h_1	R_1	a
Values (mm)	16	2	3	6	1
Parameters	b	c	d	g	
Values (mm)	6.7	1–6.7	13	1–6.0	

In this work, a novel double-layer RA employing subwavelength multi-resonant elements is proposed to achieve broadband performance in the C band. The design combines a dual-layer dielectric configuration with complementary resonant structures on separate layers to form triple-resonance characteristics. The upper layer employs circular-ring and curved delay-line elements, while the lower layer integrates Koch-fractal-inspired loops and cross-shaped patches to achieve wideband phase compensation.

https://doi.org/10.1017/S1759078726103390 Published online by Cambridge University Press

An ultra-wideband printed log-periodic dipole antenna (LPDA) serves as the feed, providing uniform amplitude distribution and reducing aperture blockage.

The remainder of this paper is organized as follows. The section on "Reflectarray element design" describes the design and operating mechanism of the proposed double-layer reflective unit. The section on "Scan parameter optimization" discusses the parameter optimization process and mutual-coupling analysis. The section on "Feed structure design" introduces the broadband LPDA feed design. The section on "Design of RA" presents the configuration of the complete reflectarray and its phase-compensation model. The section on "Design of RA" provides the simulated and measured results, followed by the conclusion in the section on "Conclusion".

Reflectarray element design

To realize broadband operation with high phase stability, a multilayer subwavelength reflective element was developed. The configuration of the proposed unit cell is illustrated in Fig. 1. It consists of two stacked dielectric substrates (PTFE, $\varepsilon_r = 2.55$) separated by an air gap. The upper substrate (thickness = 3 mm) and the lower substrate (thickness = 2 mm) are both printed with metallic patterns, while a continuous copper sheet on the bottom of the second layer serves as the ground plane. The unit-cell size is fixed at $P = 16$ mm, corresponding to approximately $0.33\lambda_0$ at 6.2 GHz, thus ensuring subwavelength spacing to suppress grating lobes and maintain accurate phase control.

The upper layer incorporates an arc-shaped delay-line structure, designed to generate controllable phase variations by tuning the arc angle α from 0° to 170°, yielding a 340° phase-shift range at 6.2 GHz. On the lower dielectric substrate, a cross-shaped resonator and a Phoenix-type square-ring resonator are printed in a crossed configuration to realize additional resonances at 4.8 and 5.2 GHz, respectively. By combining these three structures, the unit cell achieves triple-resonant characteristics that effectively broaden the usable frequency range while maintaining smooth phase dispersion.

To optimize the reflection magnitude and phase response, full-wave simulations were performed under infinite periodic boundary conditions with Floquet-mode excitation. The reflection-phase curves demonstrate that the designed unit provides a continuous 360° phase range with reflection magnitude exceeding 0.9 across the entire band of interest. The optimized geometric parameters of the proposed element are summarized in Table 1.

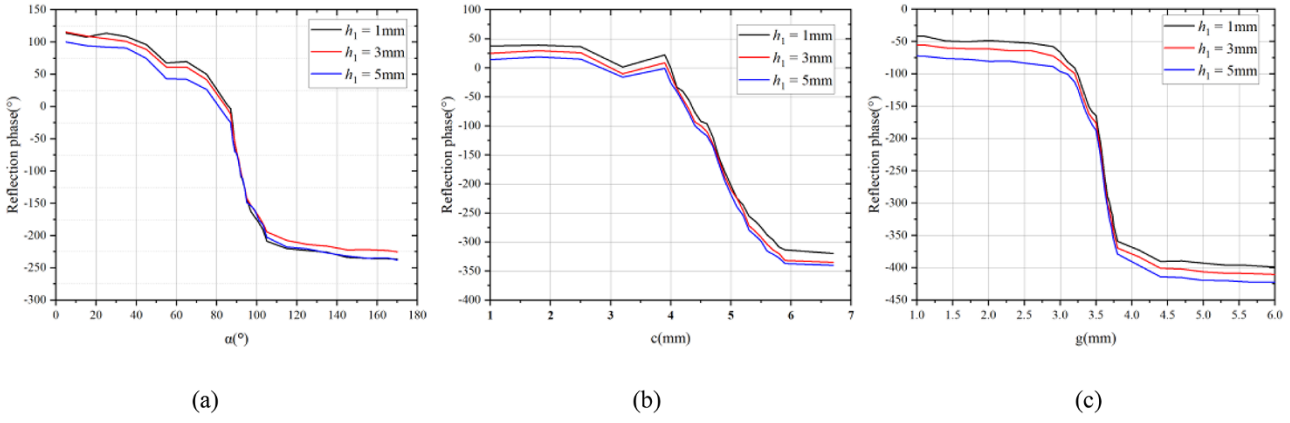


Figure 2. The phase of the reflection coefficient of the element for different values of h_1. (a) Upper ring. (b) Koch fractal. (c) Cross unit.

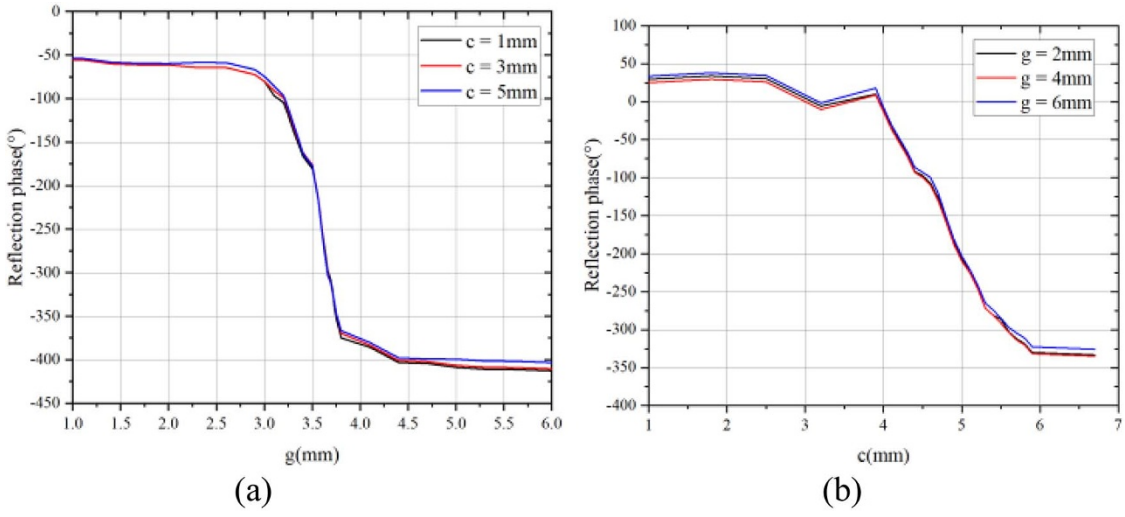


Figure 3. Mutual coupling between two elements.

https://doi.org/10.1017/S1759078726103390 Published online by Cambridge University Press

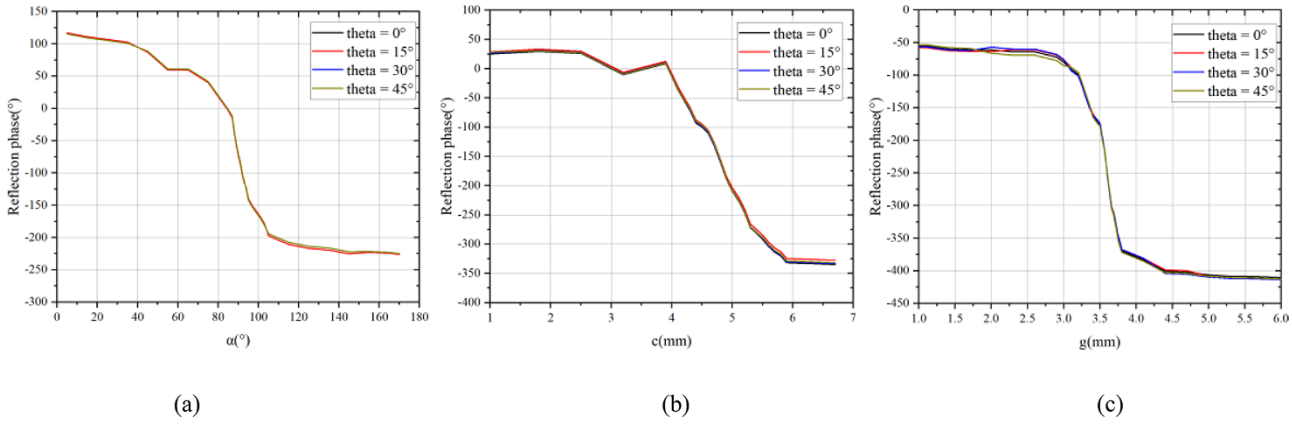


Figure 4. The phase of the reflection coefficient of the element for different incident angles theta. (a) Upper ring. (b) Koch fractal. (c) Cross unit.

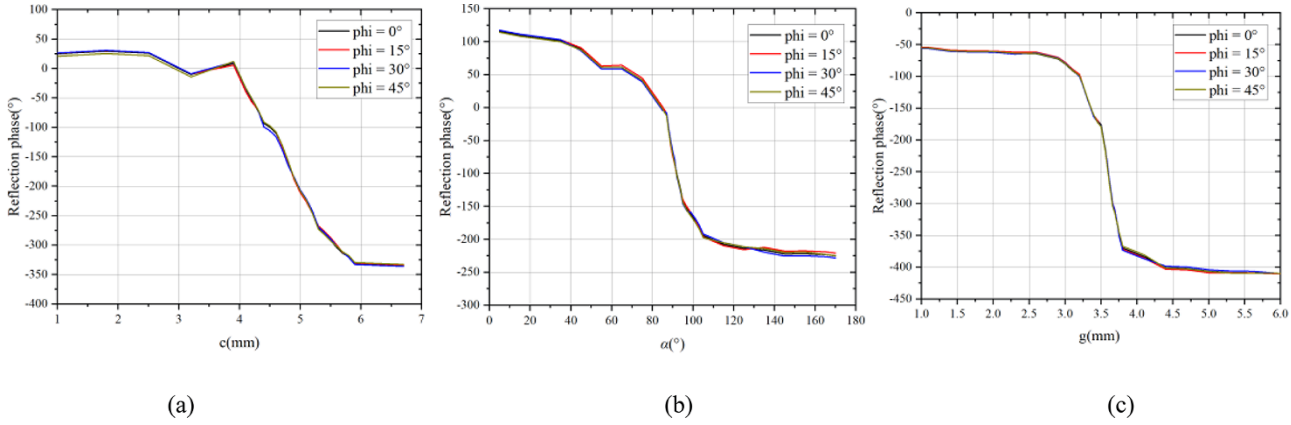


Figure 5. The phase of the reflection coefficient of the element for different incident angles phi. (a) Upper ring. (b) Koch fractal. (c) Cross unit.

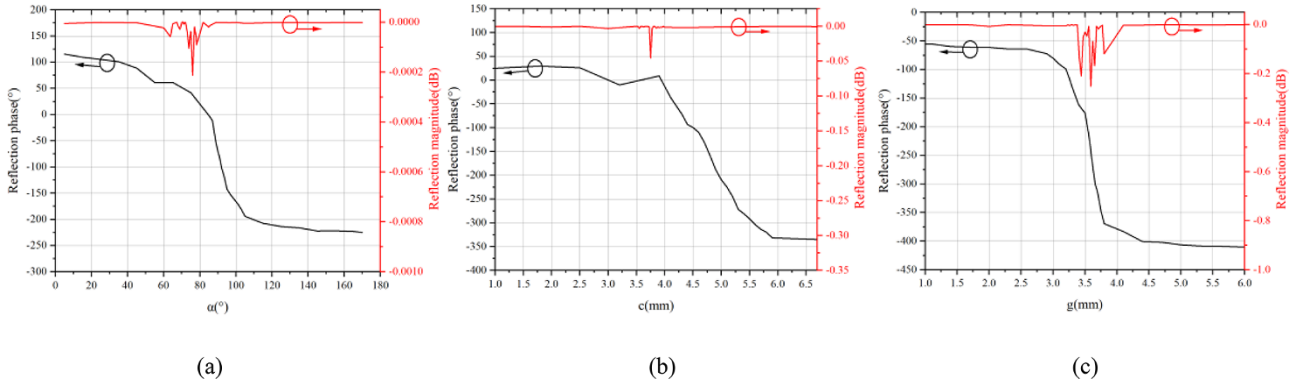


Figure 6. The phase of the reflection coefficient of the element after optimization. (a) Upper ring. (b) Koch fractal. (c) Cross unit.

Scan parameter optimization

The influence of the air-layer thickness between the two substrates on phase behavior was also investigated. As shown in Fig. 2, increasing the air gap from 1 mm to 5 mm produces a noticeable shift in the phase curve due to changes in the equivalent impedance. The optimal thickness of 3 mm was selected to achieve the best compromise between phase linearity and reflection stability.

Mutual coupling between neighboring unit cells was further analyzed using two-element periodic models shown in Fig. 3. The results indicate that the bilayer configuration effectively isolates the two resonant surfaces, minimizing coupling effects and ensuring independent phase control. Moreover, the phase-shift responses under oblique incidence ($\theta, \varphi = 0°–45°$) were examined, as shown in Figs 4 and 5. The phase deviations are maintained within ±5° over all tested incidence angles, thereby confirming the unit cell's low angular sensitivity, which is a critical requirement for practical reflectarray applications.

Finally, the optimized amplitude and phase responses of the reflective element are presented in Fig. 6. The results show that

https://doi.org/10.1017/S1759078726103390 Published online by Cambridge University Press

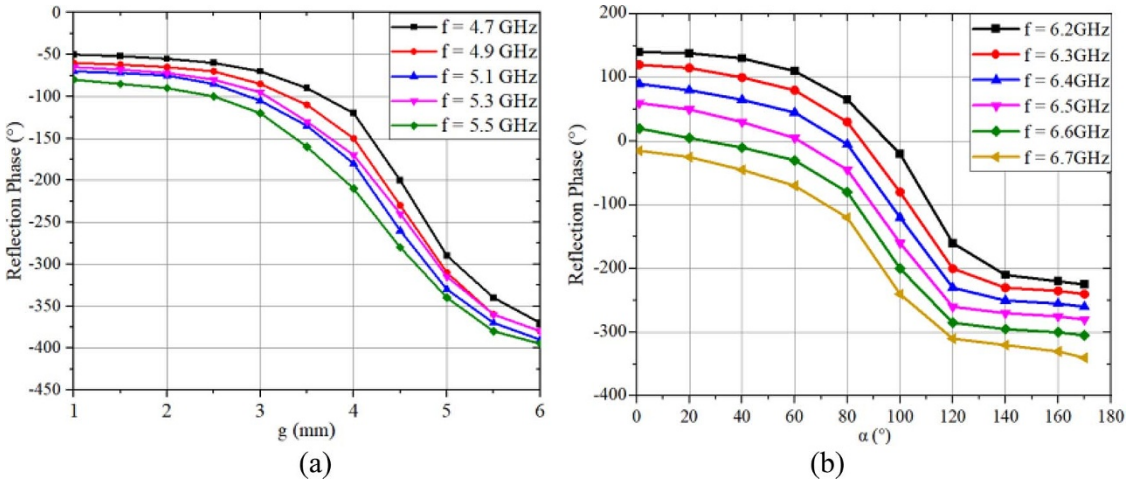


Figure 7. The phase of the reflection coefficient of the element for different frequencies. (a) Upper ring. (b) Cross unit.

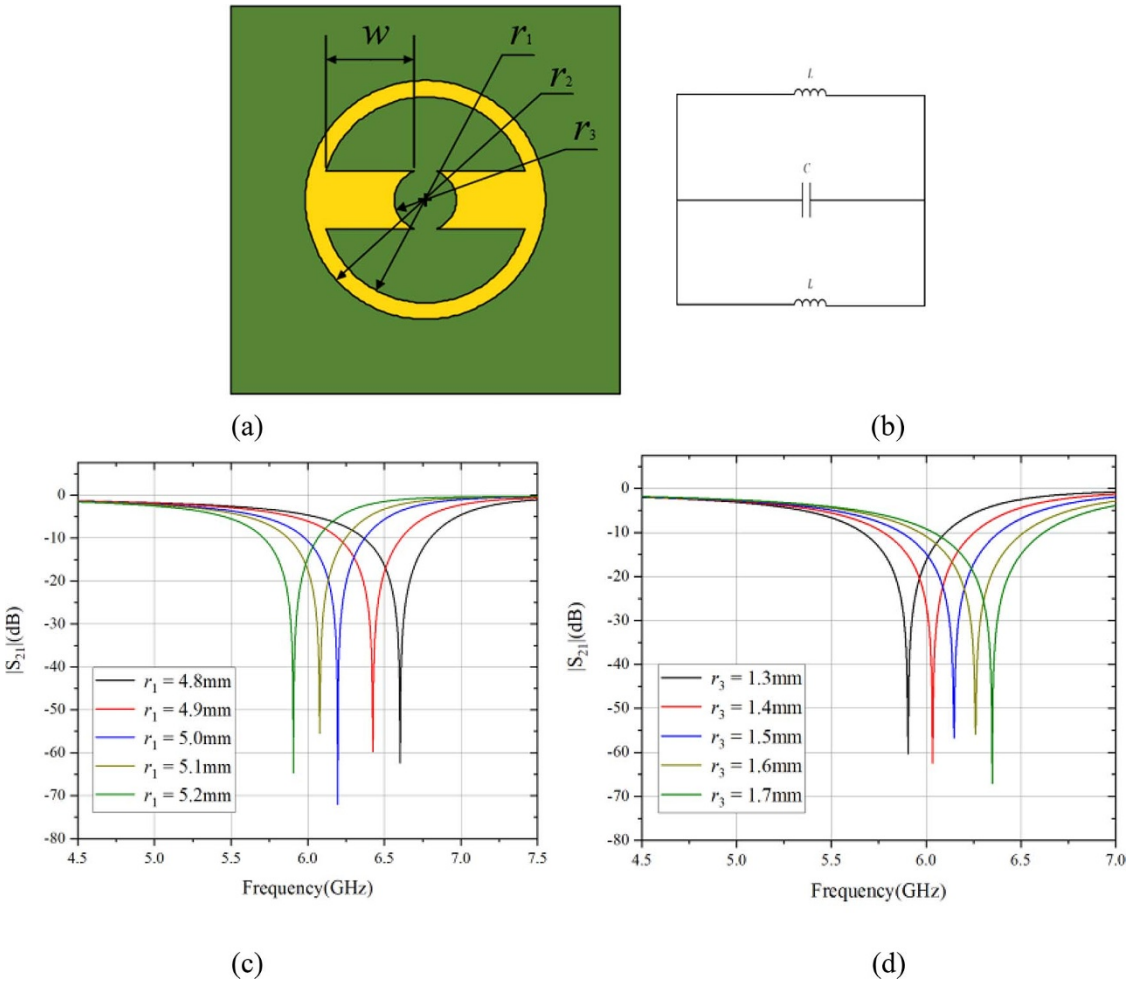


Figure 8. Transmission coefficient of FSS unit. (a) Frequency selection unit. (b) Circuit structure corresponding to frequency selection unit. (c) Under different r1-value conditions. (d) Under different r3-value conditions.

the proposed multi-resonant structure provides a full 360° phase variation while maintaining a reflection magnitude close to 0 dB. Moreover, within the operating band of 4.7–6.7 GHz, the phase response varies smoothly with the element size and exhibits an approximately linear relationship in Fig. 7. These characteristics demonstrate that the proposed unit cell can provide a broad and nearly linear phase response, which forms the basis for the proposed wideband reflectarray design.

https://doi.org/10.1017/S1759078726103390 Published online by Cambridge University Press

Table 2. Structural parameters of the FSS unit cell

Parameters	r_1	r_2	r_3	w
Values (mm)	5	6	1.5	4.2

To achieve efficient reflection at 6.2 GHz while ensuring out-of-band transmission, a series of parametric sweeps were conducted to optimize the frequency selective surface (FSS) unit cell. As illustrated in Fig. 8, the transmission characteristics are highly sensitive to the geometric parameters of the FSS. Specifically, increasing the inner radius r_1 shifts the transmission coefficient curve toward lower frequencies. When $r_1 = 5$ mm, a pronounced transmission null of −72 dB is observed at 6.2 GHz, indicating strong reflection at the desired frequency. In contrast, increasing the outer circular contour radius r_2 shifts the curve toward higher frequencies, resulting in a local transmission minimum of −56.7 dB at 6.15 GHz when $r_3 = 1.5$ mm. Considering these results, the optimal geometrical parameters were determined to be $r_1 = 5$ mm and $r_3 = 1.5$ mm to satisfy the reflection requirement at 6.2 GHz. The finalized structural dimensions are summarized in Table 2. Based on the optimized design, the FSS unit was subsequently integrated into the overall antenna configuration to verify its reflection and transmission performance.

Feed structure design

The log-periodic antenna structure consisting of multiple dipole elements arranged on a dielectric substrate is shown in Fig. 9. Designating the farthest element from the vertex as Index 1, the length of the nth symmetric dipole L_n, the spacing to its adjacent dipole x_n, and the vertical distance from the vertex y_n satisfy the following scaling relations:

$$\tau = \frac{l_{n+1}}{l_n} = \frac{x_{n+1}}{x_n} = \frac{y_{n+1}}{y_n} \tag{1}$$

The geometric scaling factor τ, typically ranging from 0.8 to 0.95, defines the periodicity of the log-periodic antenna, governing the progressive scaling of dipole lengths and spacings to

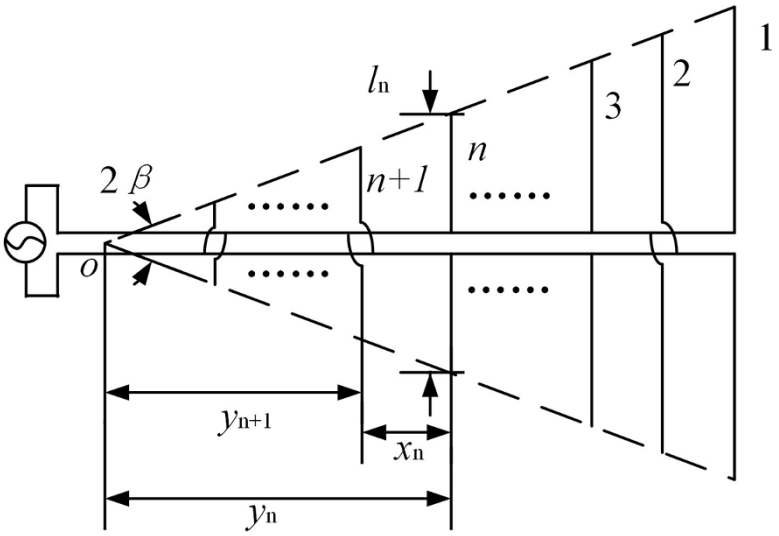


Figure 9. Logarithmic cycle antenna.

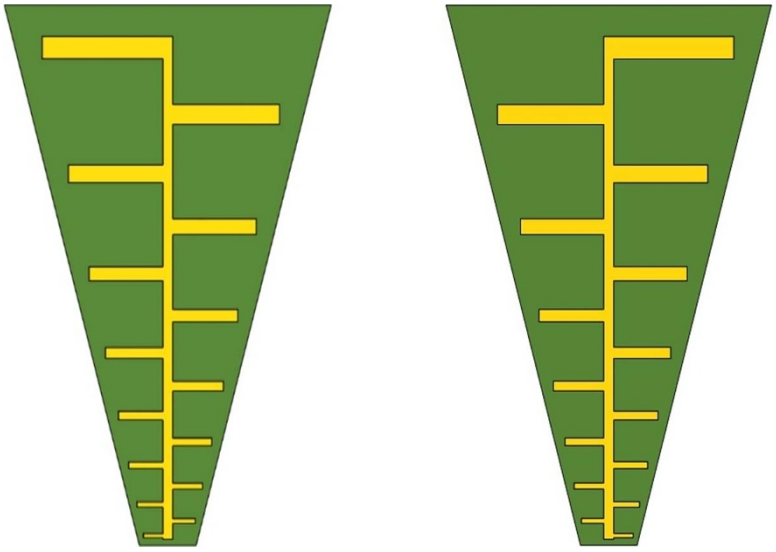


Figure 10. The structure of the Logarithmic cycle antenna as a feed.

https://doi.org/10.1017/S1759078726103390 Published online by Cambridge University Press

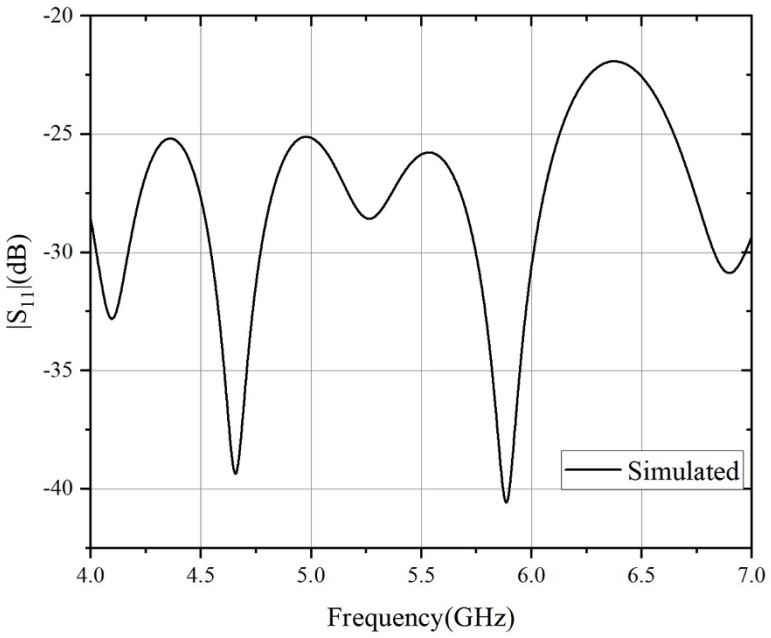


Figure 11. The reflection coefficient of the logarithmic cycle antenna.

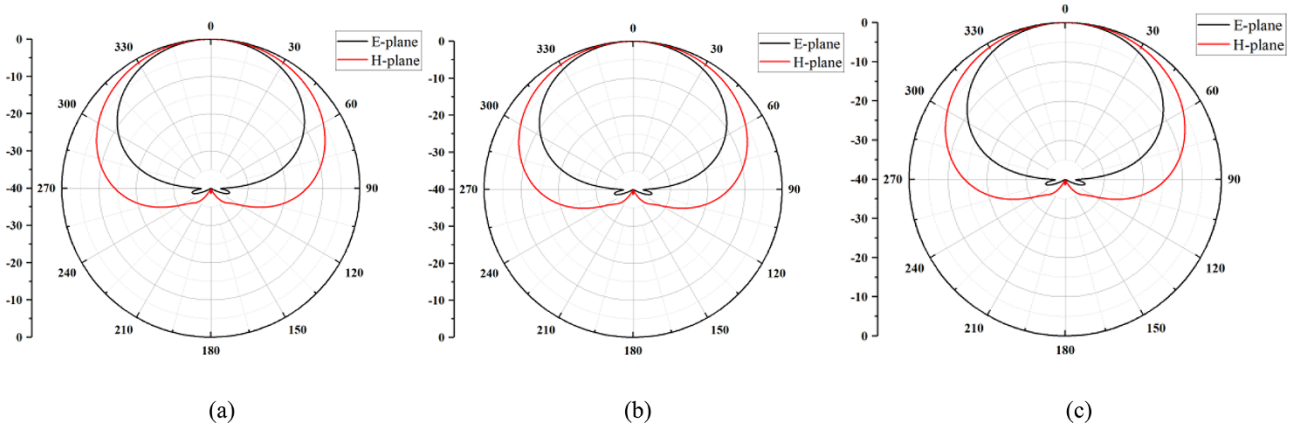


Figure 12. The radiation pattern of the logarithmic cycle antenna. (a) 4.5 GHz. (b) 5.5 GHz. (c) 6.5 GHz.

achieve frequency-independent radiation characteristics. In the above equation, the scaling factor is denoted as τ. As shown in Fig. 9, the included angle of the log-periodic antenna is 2α. For the nth symmetric dipole element, the following relationships can be derived:

$$\cot\beta = \frac{y_n}{l_n/2} \tag{2}$$

$$x_n = y_n - y_{n+1} = y_n(1-\tau) = \cot\beta\frac{l_n}{2}(1-\tau) \tag{3}$$

The proposed design employs an LPDA fabricated on an FR4 dielectric substrate with a thickness of 0.8 mm, as illustrated in Fig. 10. The antenna consists of 15 symmetrically arranged dipole elements. The longest dipole element has a length of $L_1 = 33.08$ mm and a width of $W_1 = 2.99$ mm. The antenna is fed through a parallel twin-lead transmission line with a conductor width of 1.338 mm, terminated with a matched impedance load. A cross-fed configuration is adopted, with the feed point centrally located at the shortest dipole element. Adjacent dipoles are interconnected via parallel twin-lead transmission lines to establish a 180° phase reversal, thereby ensuring that the radiation is directed from the longest toward the shortest dipole element.

Figure 11 presents the simulated reflection coefficient of the feed antenna, indicating that within the frequency range of 4–7 GHz, the reflection coefficient remains below −20 dB, which confirms excellent impedance matching across the operating band.

The radiation patterns at 4.5, 5.5, and 6.5 GHz are shown in Fig. 12, demonstrating that the beam characteristics remain largely consistent over these frequencies. Specifically, the E-plane 3-dB beamwidths are 64.7°, 96.4°, and 104.6°, while the H-plane 3-dB beamwidths are 93.1°, 96.4°, and 104.6°, respectively. In addition, the corresponding antenna gains are 8.48, 8.32, and 8.00 dBi, confirming stable radiation performance within the operating band.

Design of RA

As depicted in Fig. 13, the triple-band dual-layer microstrip reflection array antenna features a 200 mm × 200 mm aperture. The

https://doi.org/10.1017/S1759078726103390 Published online by Cambridge University Press

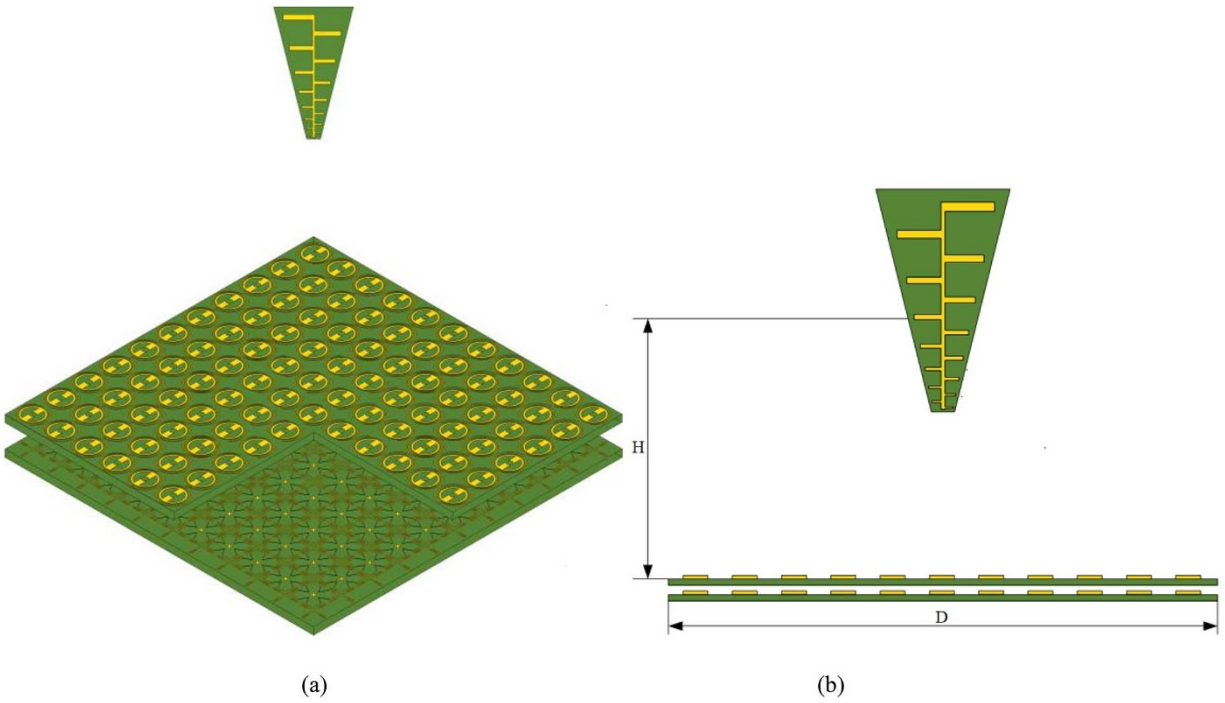


Figure 13. The configuration of the reflectarray antenna. (a) Array stereogram. (b) Array side view.

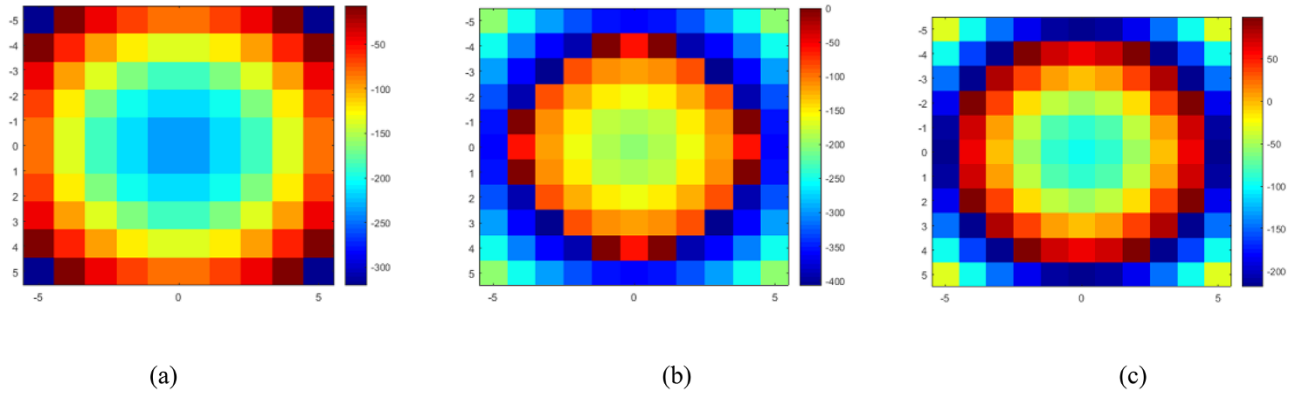


Figure 14. Phase distribution diagram. (a) Upper ring. (b) Koch fractal. (c) Cross unit.

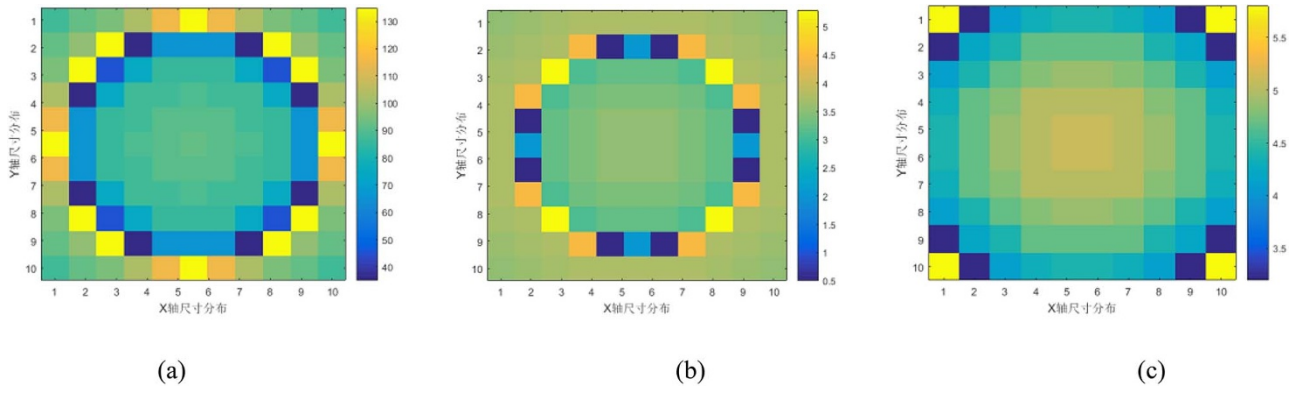


Figure 15. Unit size distribution diagram. (a) Upper ring. (b) Koch fractal. (c) Cross unit.

upper layer consists of an 11 × 11 main reflective surface array and an integrated 11 × 11 FSS. The lower layer incorporates an 11 × 11 array of cross-shaped reflection elements, which include integrated delay lines for phase control, along with a 10 × 10 array

https://doi.org/10.1017/S1759078726103390 Published online by Cambridge University Press

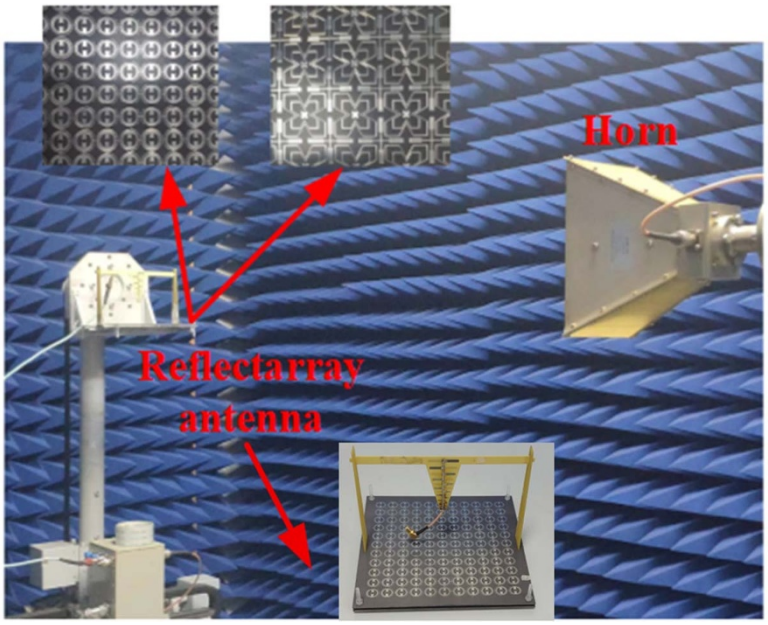


Figure 16. The fabricated reflectarray antenna and the measurement setup.

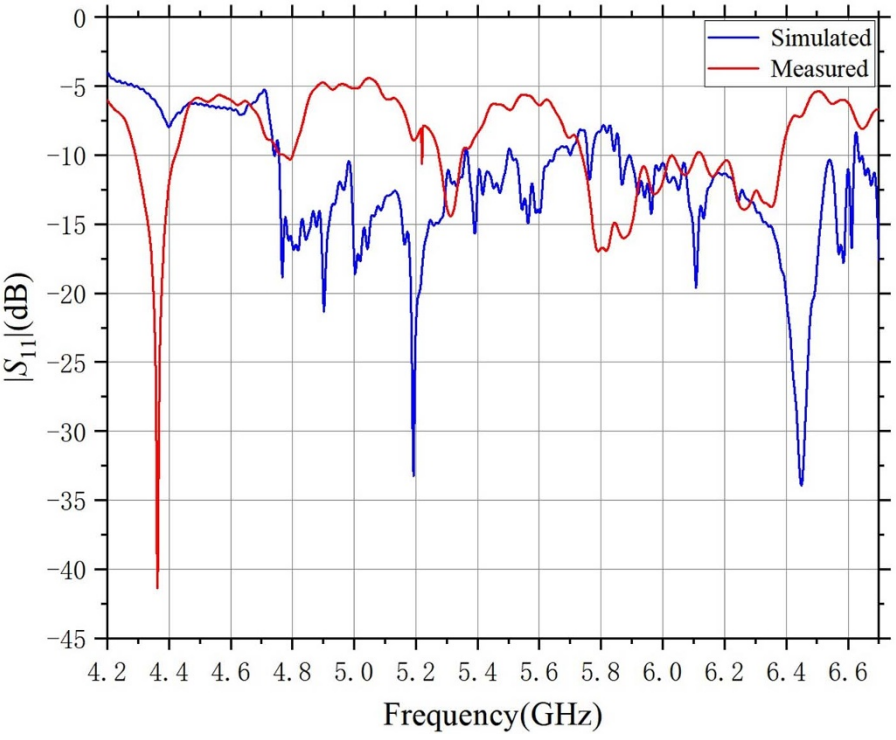


Figure 17. The measured and simulated $|S_{11}|$ of the reflection array.

of Koch fractal cyclic radiation elements. This design leverages the optimized reflection unit and logarithmic periodic feed discussed previously.

To achieve precise steering of the main beam, the compensation phase Φ_i for each array element must be calculated. The corresponding phase compensation can be expressed as

$$\phi_i = 2\pi N + k\left(R_i - \mathrm{r}_i \cdot \mathrm{r}_o\right)(N = 0, 1, 2 \ldots) \tag{4}$$

The corresponding phase compensation model for the RA involves the several parameters: k denotes the free-space wavenumber ($k = 2\pi/\lambda_0$), where λ_0 is the free-space wavelength at the central operating frequency; i represents the index of the ith radiating element within an array of N elements; R_i is the distance from the phase center of the feed antenna to the ith patch element; r_i is the position vector from the center of the planar reflectarray to the center of the ith reflective element; and r_0 defines the steering vector along the main beam direction. For the center-feed configuration with the main beam aligned along the positive z-axis, the compensation phase Φ_i can be simplified as

$$\phi_i = 2\pi N + kR_i \tag{5}$$

Empirical formulas were utilized to determine the feed height and compensation phase of each unit, resulting in the phase distribution diagram presented in Fig. 14. Additionally,

https://doi.org/10.1017/S1759078726103390 Published online by Cambridge University Press

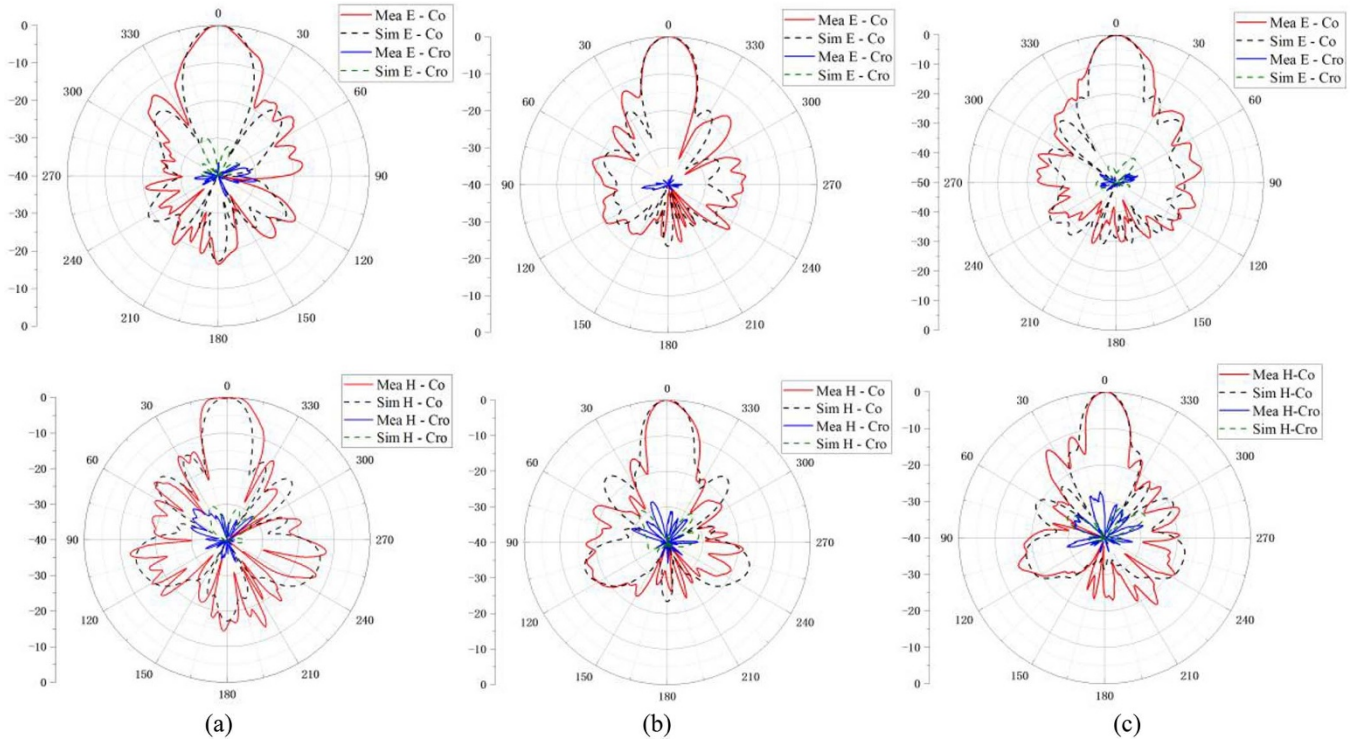


Figure 18. The E-plane patterns of the antenna and the H-plane patterns of the antenna at working frequencies. (a) 4.8 GHz. (b) 5.2 GHz. (c) 6.2 GHz.

Table 3. Performance comparison of the proposed antenna with related works

	This work	Wu et al. [7]	Luyen et al. [10]	Zhang et al. [11]
Center frequency (GHz)	4.8/5.2/6.2	15	10	37
Design mechanism	Subwavelength triple resonance	3D resonant element	Reconfigurable polarization-rotating phase shifter	Single-layer Multi-resonant
Aperture size (mm^2)	200 × 200	240 × 240	192 × 192	80 × 80
Number of elements	100/121/121	900	256	400
Phase shift range	360°/340°/355°	315°	180°	–
Peak gain (dBi)	17.1/18.7/19.9	24.5	18.5	27.86
SLL (dB)	−12.13	–	–	<−17.93
Cross-polarization level (dB)	−29.82	–	–	<−25

optimization of unit dimensions yielded the corresponding unit size distribution, as shown in Fig. 15.

Design of RA

Figure 16 shows a photograph of the test environment for the multi-frequency reflectarray. To enhance the stability of the array, Substrate-2 is secured to Substrate-1 using insulating screws. The assembly of Substrate-1 and Substrate-2 is then connected together via a bracket, the top of which is attached to the feed source. In this section, the proposed array prototype is simulated and analyzed using CST Microwave Studio, and the reflection coefficient of the simulated RA at the operating frequencies is presented in Fig. 17. As shown in the figure, the reflection coefficient remains below −10 dB over the frequency range of 4.76–6.70 GHz, indicating good impedance matching across the operating band.

The measured results indicate a noticeable frequency shift toward the lower end of the spectrum compared to the simulation. This discrepancy, along with a more pronounced performance degradation in the higher frequency band, is primarily attributed to manufacturing tolerances. These tolerances introduced slight substrate bending, which disturbed the critical impedance transformation relationship between the feed point and the fractal radiating elements. Furthermore, during measurement, the radiation from the RF cable in close proximity to the coaxial probe likely interacted with the antenna, further compromising the results.

Figure 18(a)–(c) presents the simulated E-plane radiation patterns of the proposed RA at 4.8, 5.2, and 6.2 GHz, respectively. The main beam direction remains stable across these frequencies, with sidelobe levels suppressed below −17.1, −18.3, and −15 dB, while

https://doi.org/10.1017/S1759078726103390 Published online by Cambridge University Press

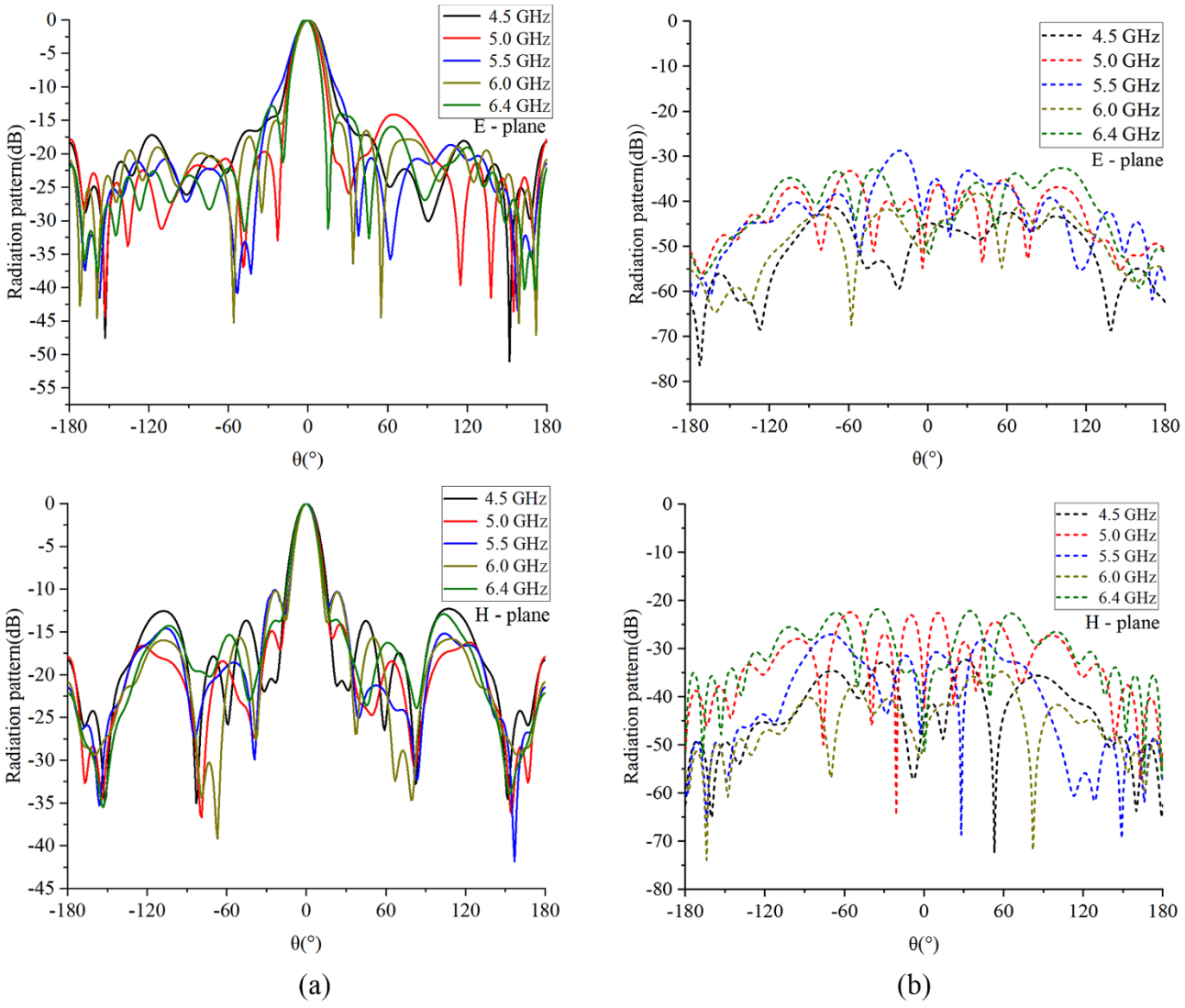


Figure 19. The E-plane patterns of the antenna and the H-plane patterns of the antenna at other frequencies. (a) Main polarization. (b) Cross-polarization.

the cross-polarization levels are consistently maintained below −30 dB at these frequencies.

Similarly, the H-plane radiation patterns, also shown in Fig. 18(a)–(c), exhibit sidelobe levels of −12.6, −14.9, and −14.3 dB at 4.8, 5.2, and 6.2 GHz, respectively. The cross-polarization levels remain below −30 dB at 4.8 and 6.2 GHz, and below −29 dB at 5.2 GHz, demonstrating good polarization purity across the operating band.

Figure 19 shows the directional map simulations of the reflect array antenna in the E-plane and H-plane at other frequencies. In the E-plane, the simulated sidelobes are on average less than −13 dB at 4.5, 5.5, 6.0, and 6.4 GHz. For the cross-polarization level of the antenna, it is less than −32 dB at these frequencies. In the H-plane, the simulated sidelobes are on average less than −10 dB, and the cross-polarization level of the antenna is on average less than −22 dB.

The simulated radiation gain performance of the reflect array antenna is depicted in Fig. 20, which demonstrates a peak gain of 19.9 dBi at 6.2 GHz, with additional gains of 17.1 dBi at 4.8 GHz and 18.7 dBi at 5.2 GHz. Furthermore, the simulated gain exceeds 16 dBi across frequencies spanning from 4.46 to 6.43 GHz, demonstrating stable performance over a 1.97 GHz operational bandwidth.

Table 3 compares the proposed reflectarray with several representative designs. The proposed antenna employs a subwavelength triple-resonant unit cell, enabling a wide phase tuning range of 360°, which is larger than that reported by Luyen et al. [10]. Meanwhile, the antenna maintains a compact aperture size of 200×200 mm^2, smaller than that reported by Wu et al. [7]. Despite the reduced aperture, the proposed design achieves peak gains of 17.1–19.9 dBi with a low cross-polarization level of −29.82 dB and a sidelobe level of −12.13 dB. These results indicate that the proposed reflectarray provides a favorable tradeoff among aperture size, phase control capability, and radiation performance.

Conclusion

A novel C-band wideband RA utilizing double-layered subwavelength elements has been presented. This antenna features an upper-layer structure comprising a frequency-selective unit with a circular ring internally connected to two open-circuited stubs and a reflecting element loaded with double-arc delay lines, while

https://doi.org/10.1017/S1759078726103390 Published online by Cambridge University Press

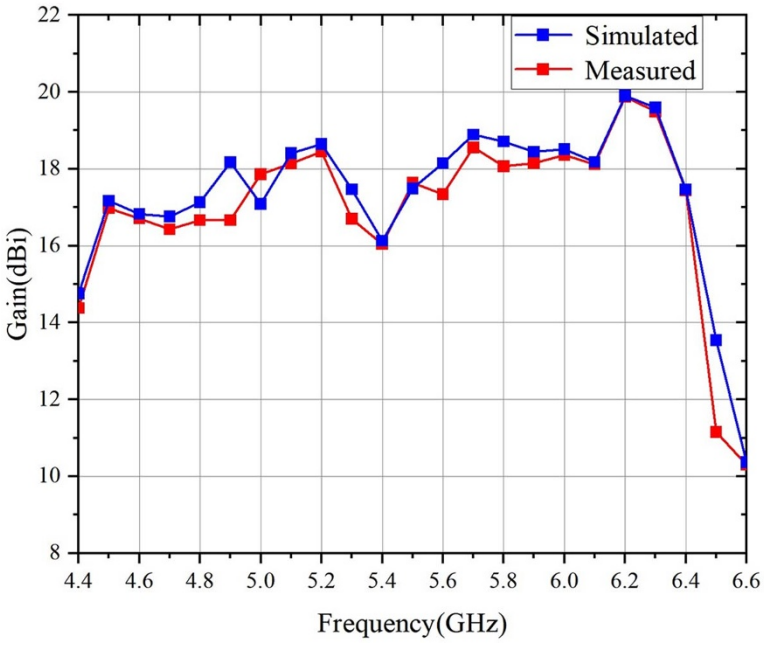


Figure 20. Simulated and measured gain of the proposed antenna.

the lower dielectric substrate integrates first-order Koch fractal-inspired Phoenix loop units and cross-shaped patch-loaded delay lines as reflecting elements; driven by an ultra-wideband log-periodic feed (centrally fed via SMA connector at the shorter dipole, radiating from the longer to the shorter dipole) for a 200 mm × 200 mm reflectarray aperture with the phase center positioned 83.7 mm above its center, it achieves a simulated −10 dB impedance bandwidth spanning 4.76–6.70 GHz, exhibits measured E-plane sidelobe levels below −12.13 dB and cross-polarization under −29.82 dB at 4.8, 5.2, 6.2 GHz, demonstrates H-plane sidelobes under −11.05 dB and cross-polarization below −27.27 dB at identical frequencies, and delivers a peak gain of 19.9 dBi at 6.2 GHz.

Funding statement. This work was supported by the National Science Foundation of China (62071282).

Competing interests. The authors report no conflict of interest.

References

1. **Munson RE, Haddad HA and Hanlen WJ** (1987) Microstrip reflectarray for satellite communication and radar cross-section enhancement or reduction. *US Patent* **4 684 952**.
2. **Huang J and Encinar JA** (2008) Introduction to reflectarray antenna, in reflectarray antennas. *IEEE*, pp. 1–7.
3. **Wang M, Li X, Hao H, Luo W, Chen Z and Tian Z** (2024) A wideband high-efficiency metal-only folded reflectarray using subwavelength detachable trapezoidal grooved element. *IEEE Transactions on Antennas and Propagation* **72**(6), 5307–5312. https://doi.org/10.1109/TAP.2024.3388211
4. **Ning Y, Zhu S, Chu H, Zou Q, Zhang C and Li J** (2024) 1-bit low-cost electronically reconfigurable reflectarray and phased array based on p-i-n diodes for dynamic beam scanning. *IEEE Transactions on Antennas and Propagation* **72**(2), 2007–2012. https://doi.org/10.1109/TAP.2023.3325650
5. **Pozar DM** (2003) Bandwidth of Reflectarrays. *Electronics Letters* **39**(21), 1490–1491. https://doi.org/10.1049/el:20030990
6. **Li W, Tu H, He Y, Zhang L, Wong SW and Gao S** (2023) A novel wideband tightly coupled dual-polarized reflectarray antenna. *IEEE Transactions on Antennas and Propagation* **71**(6), 5422–5427. https://doi.org/10.1109/TAP.2023.3262969
7. **Wu LX, Hu Q, Luo XY, Zhao J, Jiang T and Chen K** (2022) Wideband dual-feed dual-polarized reflectarray antenna using anisotropic metasurface. *IEEE Antennas and Wireless Propagation Letters* **21**(1), 129–133. https://doi.org/10.1109/LAWP.2021.3121018
8. **Zhao J, Fu C, Li H, Li F and Hu X** (2022) A single-layer broadband ka-band reflectarray using novel windmill elements. *IEEE Transactions on Antennas and Propagation* **70**(11), 11167–11171. https://doi.org/10.1109/TAP.2022.3191442
9. **Min M and Guo L** (2019) Design of a wideband single-layer reflectarray antenna using slotted rectangular patch with concave arms. *IEEE Access* **7**, 176197–176203. https://doi.org/10.1109/ACCESS.2019.2957840
10. **Luyen H, Zhang Z, Booske JH and Behdad N** (2022) Wideband, beam-steerable reflectarray antennas exploiting electronically reconfigurable polarization-rotating phase shifters. *IEEE Transactions on Antennas and Propagation* **70**(6), 4414–4425. https://doi.org/10.1109/TAP.2022.3141060
11. **Zhang YH, Dai XW, Fu YH, Tang NQ and Mi DL** (2023) A broadband multi-beam dual-circularly polarized reflect-array for Ka-band application. *IEEE Access* **11**, 48593–48600. https://doi.org/10.1109/ACCESS.2023.3276931
12. **Zhao XB, Wei F, Shi XW and Zeng C** (2021) Broadband folded reflectarray antenna using single-layer cross-polarization conversion subwavelength elements. *IEEE Antennas and Wireless Propagation Letters* **20**(4), 612–616. https://doi.org/10.1109/LAWP.2021.3059017
13. **Jost T, Wang W, Perez-fontan F and Fiebig UC** (2011) Comparison of L- and C-Band satellite-to-indoor broadband wave propagation for navigation applications. *IEEE Transactions on Antennas and Propagation* **59**(10), 3899–3909. https://doi.org/10.1109/TAP.2011.2163753
14. **Kim G, Hwang M, Jeong H, Lim C-M, Park KY and Kim S** (2022) Design of a flat-panel metasurface reflectarray C-Band antenna. *Electronics* **11**(17), 2729. https://doi.org/10.3390/electronics11172729

https://doi.org/10.1017/S1759078726103390 Published online by Cambridge University Press



Yunlong Wu received the B.E. degree in electronic information engineering from Taiyuan Institute of Technology, Taiyuan, China, in 2022. He is currently pursuing the M.S. degree with the School of Physics and Electronic Engineering, Shanxi University, Taiyuan, China. His current research interests include reflectarray antennas, wideband antennas, electrically small antennas, and metasurface-based antenna design.



Zhiyuan Yang received the B.E. degree in communication engineering from Hebei University, Baoding, China, in 2020, and the M.S. degree in communication engineering from Shanxi University, Taiyuan, China, in 2023. His research interests include antenna design, reflectarray antennas, and microwave and wireless technologies.



Yufeng Liu was born in Shanxi Lvliang, China, in 1986. He received the PhD degree in radio physics from Sichuan University, Sichuan, China,in 2014. In 2015, he joined the College of Physics and Electronic Engineering, Shanxi University. His research is mainly focused on computational electromagnetics and antenna design.

https://doi.org/10.1017/S1759078726103390 Published online by Cambridge University Press